Preview-based Asymmetric Load Reduction of Wind Turbines

Madsen, Mathias; Filsø, Jakob; Soltani, Mohsen

Published in:
IEEE International Conference on Control Applications

DOI (link to publication from Publisher):
10.1109/CCA.2012.6402671

Publication date:
2012

Document Version
Early version, also known as pre-print

Preview-based Asymmetric Load Reduction of Wind Turbines

Mathias Madsen, Jakob Filsø, and Mohsen Soltani

Abstract— **Fatigue loads on wind turbines caused by an asymmetric wind field become an increasing concern when the scale of wind turbines increases. This paper presents a model based predictive approach to reduce asymmetric loads by using Light Detection And Ranging (LIDAR) measurements. The Model Predictive Controller (MPC) developed is based on a model with individual blade pitching to utilize the LIDAR measurements. The MPC must also maintain a given power reference while satisfying a set of actuator constraints. The designed controller was tested on a 5 MW wind turbine in the FAST simulator and compared to the same controller without LIDAR data. The results showed that the MPC with LIDAR was able to reduce the asymmetric loads compared to the MPC without LIDAR while still maintaining the power reference.**

I. INTRODUCTION

The wind turbine industry has been growing rapidly over the last decade as a cause of more interest in renewable energy sources [1]. The way wind turbine manufacturers are trying to reduce the cost of energy is by expanding the size of the wind turbine structures to capture more wind energy [2]. This expansion requires the use of lighter materials which combined with the larger structure increase the flexibility of the turbine structure. The increase of blade spans of the turbines causes more asymmetry in the wind field raising the possibility for more varying turbulence affecting local areas of the rotor plane resulting in fatigue loads on the turbine structure. These factors demand more advanced control strategies to mitigate the increased loads in the structure while still maintaining the produced power at the rated level.

Traditionally, in full load operation, the collective pitch angle is adjusted to control the aerodynamic rotational torque of the rotor [3]. The input to the wind turbine that is the reference for the collective pitch angle is controlled by a PID controller, acting on the generator speed [4]. In this case, the collective pitch control is not able to reduce harmonic loads that are caused by asymmetric loads on the rotor plane. These loads normally appear as harmonics with frequency peaks at integer coefficients of the rotor angular velocity, $n \cdot P$. For a 3-bladed turbine, which is used in this paper, the asymmetric loads appear at the $1P$ frequency as well as harmonics with frequency peaks at integer coefficients of $3P$, $6P$, $9P$ etc. For large scale wind turbines, the loads at the $1P$ frequency contribute very significantly to the fatigue loads on the structural components of the wind turbine, and is therefore of great interest [5]. The works in [6], [7], and [8] show that the $1P$ frequency loads can be reduced by adding a correction to the reference command of individual pitch references.

In this paper, we show that by using Light Detection and Ranging (LIDAR), which provides preview information of the wind field for the wind turbine controller, a reduction of the $1P$ frequency harmonic loads is achieved. In [9], [10], and [11] the LIDAR preview information showed to have a big potential for reduction of loads in wind turbine structures. However, these works use only simple models for designing a collective pitch controller. In this paper, we propose a model-based design of a predictive controller which incorporates the preview information as an input to the individual pitch controller. The controller chosen is a Model Predictive Controller (MPC), as actuator constraints and preview information are easily implemented in MPC. We compare the results of the proposed controller to the MPC without LIDAR information in the high fidelity aero-servo-elastic wind turbine simulation software FAST [12] from the National Renewable Energy Laboratory (NREL) on a fictive 3-bladed 5 MW reference turbine [13].

This paper is organized as follows: Section 2 describes the modeling wind turbine, linearization hereof, and the LIDAR module. The proposed controller is forumlated in section 3, and comparison of the results are discussed in section 4. Finally, a conclusion on the paper is given in section 5.

II. WIND TURBINE MODEL

A. Aerodynamics

The aerodynamics of a wind turbine capture the wind energy and converts it into rotational energy through the blades. The rotor blades of the wind turbine are excited by the wind field which gives rise to forces and moments upon the structure and mechanical components of the turbine. The blade forces and moments are calculated for the blades individually as the wind field can vary greatly over the rotor span, thereby utilizing the information of the wind field ahead of the turbine and the blades can be controlled individually. This is done by using Blade Element Momentum (BEM) theory [14]. In BEM theory each blade is split into a number of annular blade elements N_B with seperate aerodynamic properties. Forces and moments are then found using momentum theory on each element. BEM theory uses the assumption that there are no annular aerodynamic interaction between the blade elements.

The division of a blade into a finite number of elements is shown in Fig. 1, where r_j is the distance from the hub

M. Madsen and J. Filsø were M.Sc. students at the Department of Electronic Systems, Aalborg University, 9220 Aalborg OE, Denmark. E-mail: {mbma07, jfilso07}@student.aau.dk

M. Soltani is with the Department of Electronic Systems, Aalborg University, 9220 Aalborg OE, Denmark. E-mail: sms@es.aau.dk

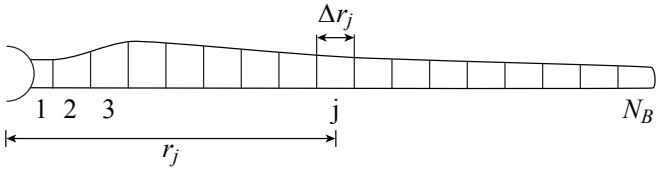

Fig. 1. Decomposition into blade elements. The distance r_j is from the hub center to the center of the j'th element and Δr_j is the length of the j'th element.

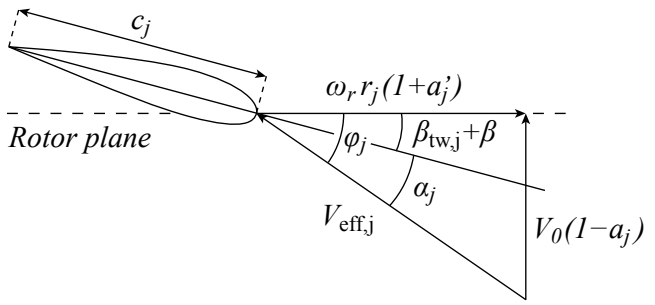

Fig. 2. Wind components and angular quantaties for blade element j.

center to the center of the j'th element and Δr_j is the length of the j'th element.

The incoming relative horizontal wind speed V_0 that the wind turbine experiences is dependent on the horizontal tower velocity $\dot{x}_t$ in the downwind direction (see Fig. 3), and is given by $V_0 = V_w - \dot{x}_t$, where V_w is the horizontal free stream wind speed.

The effective wind speed that each blade element is exposed to depends on the angular velocity of the rotor ω_r, together with two induction factors that capture the effect of the presence of the blade elements. The axial induction factor a_j and the tangential induction factor a'_j describe the change in horizontal wind speed and the change in tangential wind speed for the j'th element, respectively. Effective wind speed is then given by

$$V_{\text{eff,j}} = \frac{V_0(1-a_j)}{\sin(\phi_j)} = \frac{\omega_r r_j(1+a'_j)}{\cos(\phi_j)}, \tag{1}$$

where the local inflow angle ϕ_j is the angle between the effective wind speed and the rotor plane as shown in Fig. 2.

The local angle of attack shown in Fig. 2 is defined as $\alpha_j = \phi_j - \beta_{\text{tw,j}} - \beta$, where $\beta_{\text{tw,j}}$ is the local twist angle of the blade element and β is the pitch angle of the entire blade.

Lift and drag forces on a blade element, L_j and D_j, are found using coefficient curves $C_{l,j}(\alpha_j)$ and $C_{d,j}(\alpha_j)$ and are given by

$$\begin{aligned} L_j &= \frac{\rho}{2} V_{\text{eff,j}}^2 c_j C_{l,j}(\alpha_j) \\ D_j &= \frac{\rho}{2} V_{\text{eff,j}}^2 c_j C_{d,j}(\alpha_j), \end{aligned} \tag{2}$$

where ρ is the density of the air, c_j is the chord length of the j'th element shown in Fig. 2. The drag force points in the direction of the effective wind speed and the lift force is perpendicular to it.

The rotational torque T_r, tangential bending moment M_b, and thrust force F_t for a single blade, which are of interest in this paper, are now found by summation of the contributions from each blade element given by

$$\begin{aligned} T_r &= \sum_{j=1}^{N_B} \left(L_j \sin(\phi_j) - D_j \cos(\phi_j)\right) r_j \Delta r_j \\ M_b &= \sum_{j=1}^{N_B} \left(L_j \cos(\phi_j) + D_j \sin(\phi_j)\right) r_j \Delta r_j \\ F_t &= \sum_{j=1}^{N_B} \left(L_j \cos(\phi_j) + D_j \sin(\phi_j)\right) \Delta r_j. \end{aligned} \tag{3}$$

To calculate (3) for a given wind speed, rotational speed, and blade pitch angle, the local inflow angle, axial induction factor, and tangential induction factor are needed for each element. By rewriting (1) the local inflow angle is obtained by

$$\phi_j = \arctan\left(\frac{(1-a_j)V_0}{(1+a'_j)\omega_r r_j}\right). \tag{4}$$

Thus, the local inflow angle is dependent on the induction factors. These are expressed as

$$a_j = \left(\frac{4F\sin(\phi_j)^2}{\sigma_j C_n} + 1\right)^{-1} \tag{5}$$

$$a'_j = \left(\frac{4F\sin(\phi_j)\cos(\phi_j)}{\sigma_j C_t} - 1\right)^{-1}, \tag{6}$$

where F is the Prandtl approximation for tip and root loss factors [14], σ_j is the solidity which is the fraction of the annular area that the blades at the local radius are sweeping. C_n and C_t are the axial and tangential force coefficients respectively, given by

$$\begin{aligned} C_n &= C_l(\alpha)\cos(\phi_j) + C_d(\alpha)\sin(\phi_j) \\ C_t &= C_l(\alpha)\sin(\phi_j) - C_d(\alpha)\cos(\phi_j). \end{aligned} \tag{7}$$

As seen, the induction factors are dependent on the local inflow angle and vice versa. These are calculated by initializing the induction factors to zero, and then calculating the local inflow angle by (4). This first estimate is then used to calculate the induction factors by (5) and (6). This proces is repeated until the changes in inflow angle and induction factors become sufficiently small.

B. Structure Dynamics

The asymmetric loads are described by transforming the three tangential blade moments M_{b1}, M_{b2}, and M_{b3} into a non-rotating coordinate system by the Coleman transform [15]. Two of the three coordinates of the non-rotating coordinate system are used. These describe the rotor tilt and yaw moments given by

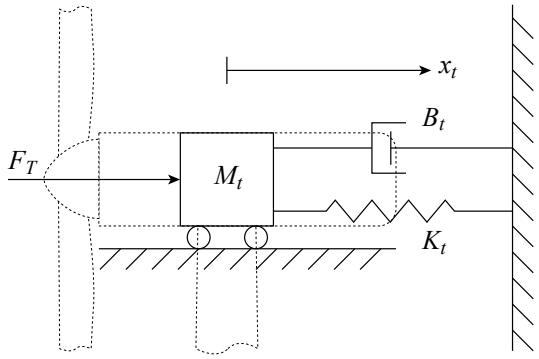

Fig. 3. Lumped representation of the wind turbine fore-aft tower deflection. The tower deflection x_t is positive in the downwind direction.

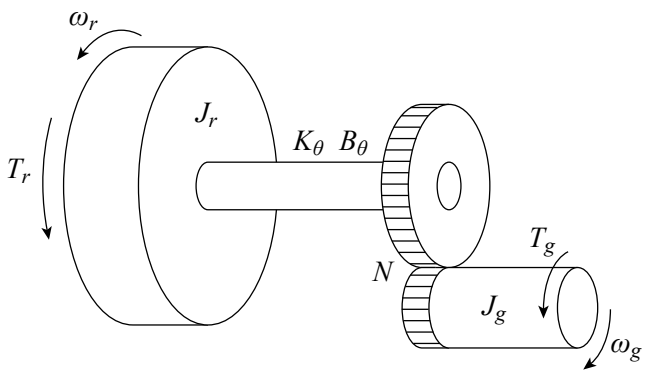

Fig. 4. Lumped representation of the wind turbine drivetrain dynamics. The angular velocities ω_r and ω_g have opposite positive directions.

$$\begin{bmatrix} M_t \\ M_y \end{bmatrix} = T_c \begin{bmatrix} M_{b1} \\ M_{b2} \\ M_{b3} \end{bmatrix}, \tag{8}$$

where M_t and M_y are tilt and yaw moments respectively, and T_c is the Coleman tranformation matrix. The transformation matrix T_c is given by

$$T_c = \frac{2}{3} \begin{bmatrix} \cos(\psi) & \cos\left(\psi + \frac{2\pi}{3}\right) & \cos\left(\psi + \frac{4\pi}{3}\right) \\ \sin(\psi) & \sin\left(\psi + \frac{2\pi}{3}\right) & \sin\left(\psi + \frac{4\pi}{3}\right) \end{bmatrix}, \tag{9}$$

where ψ is the azimuth angle of the first blade as shown in Fig. 5.

The thrust force from the rotor is transferred to the structure of the wind turbine. This results in a fore-aft deflection of the tower. The fore-aft motion of the tower x_t is expressed as a second-order linear translational model as shown in Fig. 3 and is given by

$$\ddot{x}_t(t) M_t = F_T(t) - K_t x_t(t) - B_t \dot{x}_t(t), \tag{10}$$

where M_t is the equivalent mass of the tower, B_t is the damping coefficient, and K_t is the stiffness.

C. Drivetrain, Generator, and Pitch Actuator

The drivetrain transfers the rotor torque T_r to the generator which in turn transforms it to electrical power by applying a generator torque T_g. A visual representation of the drivetrain is shown in Fig. 4. As traditional generators operate at higher rotational speeds than the rotor, a gearing between the rotor and the generator is used. The rotor is mounted on a shaft usually termed the low-speed shaft which connects to the high-speed shaft of the generator through the gearing.

The drivetrain is modeled by two inertias: One at the low-speed shaft J_r and one at the high-speed shaft J_g. A rotational damping B_θ and a rotational stiffness K_θ are added to the low-speed shaft to model the shaft torsion θ. The equations for the drivetrain are given by

$$\begin{aligned} \dot{\omega}_r(t) J_r &= T_r(t) - K_\theta \theta(t) - B_\theta \dot{\theta}(t) \\ \dot{\omega}_g(t) J_g &= -T_g(t) + \frac{K_\theta}{N} \theta(t) + \frac{B_\theta}{N} \dot{\theta}(t) \\ \dot{\theta}(t) &= \omega_r(t) - \frac{\omega_g(t)}{N}, \end{aligned} \tag{11}$$

where ω_g is the angular velocity of the high-speed shaft and N is the gear ratio.

The generator electrical power output is controlled by the applied generator torque T_g. The generator torque is modeled by introducing the constraints

$$\begin{aligned} T_{\mathrm{gmin}} \leq T_g(t) \leq T_{\mathrm{gmax}} \\ |\dot{T}_g(t)| \leq T_{\mathrm{grate}}, \end{aligned} \tag{12}$$

where T_{gmin} is the minimum generator torque, T_{gmax} is the maximum generator torque, and T_{grate} is the slew rate of the generator torque.

The produced electrical power P_e is described by

$$P_e(t) = T_g(t) \omega_g(t) \eta_g, \tag{13}$$

where η_g is the generator efficiency.

The pitch actuators of the wind turbine use a closed loop servo system that guarantees that the pitch reference is obtained. This is modeled as a first order closed loop system given by

$$\dot{\beta}_i(t) = \frac{1}{\tau_\beta} \left(\beta_{\mathrm{ref,i}}(t) - \beta_i(t) \right), \quad i = 1, 2, 3, \tag{14}$$

subject to the constraints

$$\begin{aligned} \beta_{\min} \leq \beta_i(t) \leq \beta_{\max} \\ |\dot{\beta}_i(t)| \leq \beta_{\mathrm{rate}}, \end{aligned} \tag{15}$$

where τ_β is the time constant of the pitch system, $\beta_{\mathrm{ref,i}}$ is the pitch angle reference for the i'th blade, β_i is the pitch angle of the i'th blade, $\beta_{\min}$ and $\beta_{\max}$ are the minimum and maximum blade pitch angle, respectively, and β_{rate} is the pitch slew rate.

D. Linearization

The models of the subsystems are collected into a nonlinear state-space model

$$\dot{x}_n = f(x_n, u_n, d_n) \tag{16}$$

$$z_n = h(x_n, u_n, d_n), \tag{17}$$

where $x_n = (x_t,\ \dot{x_t},\ \omega_r,\ \omega_g,\ \theta,\ \beta_1,\ \beta_2,\ \beta_3)^T$ is the state vector, $u_n = (\beta_{\mathrm{ref},1},\ \beta_{\mathrm{ref},2},\ \beta_{\mathrm{ref},3},\ T_g)^T$ is the input vector, $d_n = (V_1,\ V_2,\ V_3)^T$ is the disturbance vector (V_1, V_2, and V_3 denote the blade wind speeds at 75 % blade span), and $z_n = (P_e,\ \beta_1,\ \beta_2,\ \beta_3,\ \dot{\beta}_1,\ \dot{\beta}_2,\ \dot{\beta}_3,\ \dot{x}_t,\ \omega_r,\ \dot{\theta},\ M_{b1},\ M_{b2},\ M_{b3})^T$ are the performance outputs used for MPC.

The aerodynamic model of the wind turbine is highly nonlinear and is not suited for control purposes. A linearized model of (16) and (17) is therefore derived. The steady state operating points used for the linearization are found by maximizing the power output at low wind speeds. In full load operation the pitch angle operating points are found by limiting the power to the rated level. Since the aerodynamics are not in closed-form expressions, the linearized aerodynamic model is derived numerically at the operating points in the dependent variables β_i, ω_r, and V_i. The expression for the generated electrical power in (13) is linearized using a first-order Taylor approximation.

As the operating point for the electrical power (and thus all operating points) are dependent on the mean wind speed $\overline{V}$, the linear model is parameterized by the mean wind speed by

$$\dot{x} = A(\overline{V})x + B_u(\overline{V})u + B_d(\overline{V})d \tag{18}$$

$$z = C_z(\overline{V})x + D_u(\overline{V})u + D_d(\overline{V})d, \tag{19}$$

where the variables x, u, d, and z denote the pertubations from the operating points. A, B_u, B_d, C_z, D_u, and D_d are the linear parameter varying state-space matrices. The reason for the independence from the azimuth angle ψ used in (9) is that neither M_t nor M_y is included in the performance outputs z, but are both instead included in the cost function in MPC by the Coleman transformation (through the weighting matrix Q) as will be explained in section 3.

E. LIDAR

The objective of the LIDAR is to provide a wind preview for each of the three blades. A wind preview at each controller time step over the entire prediction horizon of the MPC is required. The LIDAR type considered for this paper is a hub mounted Continuous-Wave LIDAR taking rotary measurements at 75 % of the blade span where the maximum power extraction from the wind is [16]. Three measurements are taken at each time step, one for each blade.

The focal distance of the measurements is chosen according to [17], which recommends that the measurement angle should be less than 45°. Given the focal distance D and a mean wind speed $\bar{V}$, the preview time T_p is calculated as $T_p = \frac{D}{\bar{V}}$. The focal distance is chosen to be 54 m, corresponding to a preview time T_p of 3 seconds for a wind field with a mean wind speed of 18 m/s (which is used in the simulations).

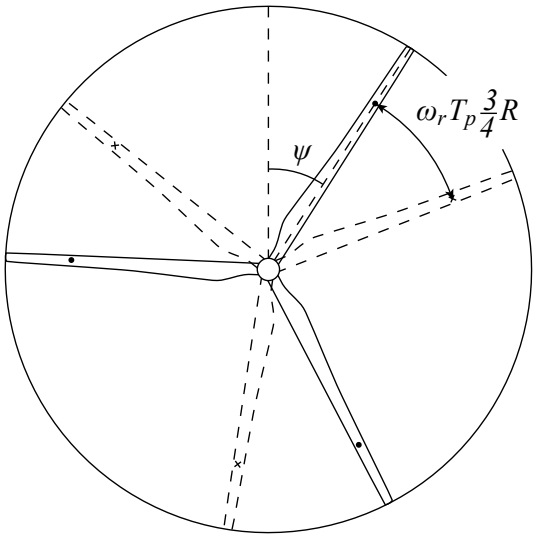

Fig. 5. LIDAR measurement positions (crosses) in the rotor plane. Measurements are taken $\omega_r T_p$ radians ahead of the blades and at 75 % blade span.

When obtaining a time history of the wind speeds, the predicted positions of the blades need to be taken into account. Because of this, the position of the measurements in the rotor plane is $\omega_r T_p$ radians ahead of each blade. This is shown in Fig. 5.

Some assumptions need to be made in order to use LIDAR for predictive control:

- The mean wind direction is perfectly aligned with the wind turbine, meaning that the lateral and vertical wind speeds both have zero mean in the preview horizon. If this is not the case, the LIDAR could be measuring entirely different speeds than those affecting the turbine.
- Turbulence moves with the mean wind speed and direction and the turbulence does not grow or fade in the preview horizon (Taylor's Frozen Turbulence Hypothesis).
- As the LIDAR measures in Line Of Sight (LOS) direction, the wind vector needs to be projected into the horizontal component of the wind. If lateral and vertical components of the wind field are present, this will give an error in the measured horizontal wind speed. It is assumed that the vertical and lateral components of the wind field are negligible compared to the horizontal component so that this error becomes very small.

Investigation of these assumptions in different LIDARs is the current topic of research, since the LIDAR technology is not mature [17].

III. CONTROLLER

The goal of this paper is to reduce the $1P$ frequency harmonic loads in the structure caused by an asymmetric wind field, while maintaining the power production at a rated level. The use of preview measurements of the wind

together with hard constraints on the system makes Model Predictive Control (MPC) well suited for this task as it provides a natural formulation of these. MPC works by predicting the future system outputs over a prediction horizon H_p and computing the optimal control inputs over a control horizon H_u. The first calculated control input is applied to the system, the horizons are then shifted one time step and the optimization is repeated for the next time step. Thus, an optimization problem is solved at each controller time step. MPC is usually formulated with a quadratic cost function and linear inequality constraints [18], as is the case for this paper. The cost function used in this paper is described by

$$\begin{aligned} J_z(k) &= \sum_{i=0}^{H_p} \|\hat{z}(k+i|k) - r(k+i)\|_Q^2 \\ J_u(k) &= \sum_{i=0}^{H_u-1} \|\hat{u}(k+i|k)\|_R^2 \\ J(k) &= J_z(k) + J_u(k), \end{aligned} \tag{20}$$

where J_z is the tracking error cost, J_u is the input cost, J is the total cost, $\hat{z}$ are the predicted outputs, r is the reference trajectory, $\hat{u}$ are the predicted inputs, Q is the output weighting matrix and R is the input weighting matrix. The predicted outputs $\hat{z}$ are calculated using (19). The reference trajectory is chosen to be a constant reference, and since the model is linearized at the operating points, the reference trajectory becomes zero for all outputs. The constraints in this paper are on the actuators. All constraints are linear and are given in (12) and (15).

Since the goal among others is to reduce the harmonic loads and the formulation of these are nonlinear in ψ, as shown in (9), they cannot be used as outputs of the linear model without scheduling very frequently. Instead they are introduced through the output weighting matrix Q. As the cost function is quadratic the tilt and yaw moments must be defined as quadratic terms as well. The sum of the squares of the tilt and yaw moments yields

$$M_t^2 + M_y^2 = \begin{bmatrix} M_{b1} & M_{b2} & M_{b3} \end{bmatrix} \mathcal{T} \begin{bmatrix} M_{b1} \\ M_{b2} \\ M_{b3} \end{bmatrix}, \tag{21}$$

where $\mathcal{T} = T_c^T T_c$. The matrix $\mathcal{T}$ is positive-semidefinite as it is a requirement for Q. By using trigonometric identities, $\mathcal{T}$ is further reduced to

$$\mathcal{T} = \frac{2^2}{3^3} \begin{bmatrix} 1 & -\frac{1}{2} & -\frac{1}{2} \\ -\frac{1}{2} & 1 & -\frac{1}{2} \\ -\frac{1}{2} & -\frac{1}{2} & 1 \end{bmatrix}, \tag{22}$$

which shows that $\mathcal{T}$ is constant and independent from ψ. The output weighting matrix Q is now expressed as

$$Q = \begin{bmatrix} \mathrm{I} & 0 \\ 0 & \mathcal{T} \end{bmatrix} Q_w, \tag{23}$$

where I is the identity matrix and Q_w is a diagonal matrix containing the weights of each output. The squared tilt and yaw moments are now included in the cost function and are independent from ψ which makes the MPC problem less complicated since a prediction of ψ is not needed to generate output weighting matrices for each time step in the prediction horizon. Instead Q is constant over the entire prediction horizon.

The MPC is designed with weights on the performance outputs as well as the inputs given in section 2. The MPC controller is implemented with a sample rate of 10 Hz, prediction horizon of 15 and a control horizon of 15.

IV. RESULTS

The designed individual pitch MPC with LIDAR is compared to an MPC with collective pitch and without LIDAR measurements. Both the controllers are linearized around the mean wind speed of the test wind field, and full state information is assumed in the simulation. The wind field is generated with the stochastic wind field simulator TurbSim from NREL [19]. The generated wind field measured at the hub is shown in Fig. 6.

The primary goal is to produce power and keep the power production steady at the rated level. The comparison of the power production is shown in Fig. 7. It is seen that both controllers are able to maintain the rated power level (5 MW). However the power of the MPC with LIDAR has a slightly lower sample standard deviation of 0.29 % compared to 0.36 % for the MPC without LIDAR.

To compare the asymmetric loads of the controllers, the power spectral densities of the flap-wise bending moment of blade 1 and the bending moment of the low-speed shaft at the tip (in the direction of blade 1) are shown in Fig. 9 and 10, respectively. Both figures show significant reductions around the $1P$ frequency (0.2 Hz) of the LIDAR based MPC compared to the MPC without LIDAR. The reduction for the shaft bending moment is 85 % and the reduction for the flap-wise blade bending moment is 60 %.

Furthermore the damage equivalent load (DEL) reduction for the shaft bending moment at the tip, flap-wise bending moment for blade 1 and tower deflection are calculated using the rainflow counting algorithm according to [20]. The reduction of the shaft bending DEL is 33.9 %, the flap-wise

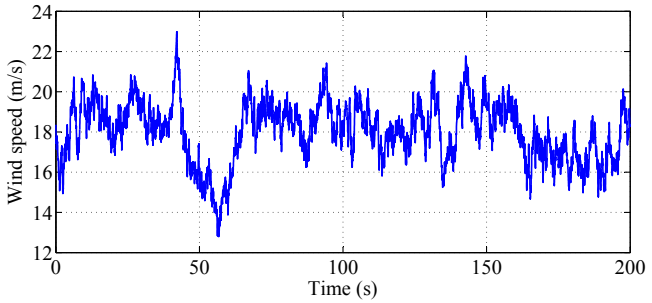

Fig. 6. Simulation wind speed measured at the hub.

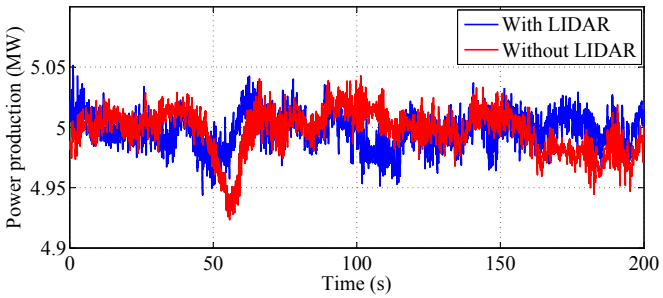

Fig. 7. Power production comparison of MPC and baseline controller.

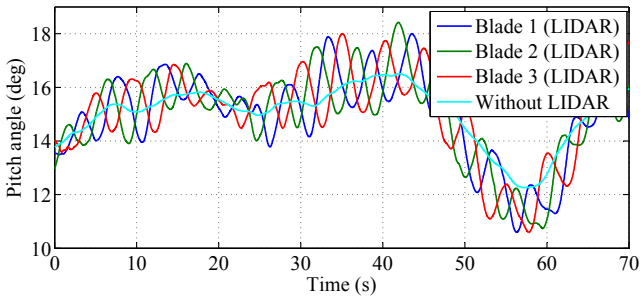

Fig. 8. Comparison of pitch activity from 0 s to 70 s.

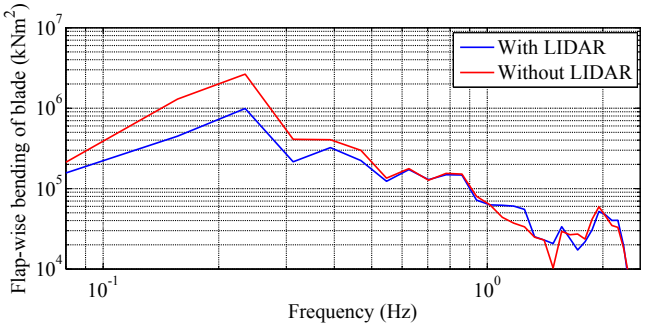

Fig. 9. Power spectral density of flap-wise bending moment of blade 1.

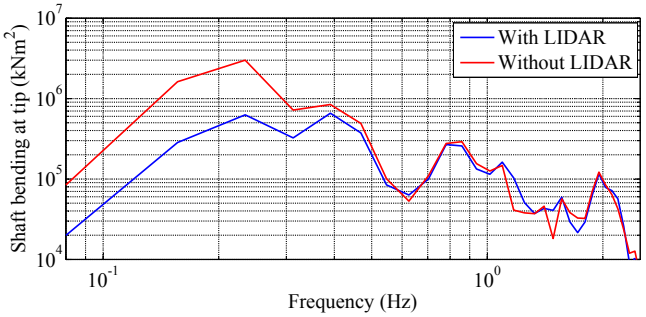

Fig. 10. Power spectral density of the moment at the tip of the low-speed shaft in a rotating coordinate system pointing in the direction of blade 1.

bending DEL reduction is 11.6 %, and the tower deflection DEL is reduced by 15.6 %.

The pitch activity of both controllers is shown in Fig. 8. As seen, the LIDAR based MPC introduce harmonic motions in the pitch actuators to counteract the harmonic $1P$ moments.

V. CONCLUSION

The goal of this paper was to show the possibility of using LIDAR to reduce harmonic loads caused by an asymmetric wind field while maintaining a power reference. This was done by using MPC with LIDAR measurements. A model with individual blade pitching was developed for MPC and parameterized by the mean wind speed. Non-rotating tilt and yaw moments were introduced to the cost function of MPC to reduce the harmonic loads. The power was maintained at the rated level, while greatly reducing the power of the harmonic loads of both the low-speed shaft bending moment and the flap-wise blade bending moment around the $1P$ frequency by 85 % and 60 %, respectively.

REFERENCES

[1] BTM Consult, "World Market Update 2010. Forecast 2011-2015," *International Wind Energy Development*, 2010.

[2] F. D. Bianchi, H. De Battista, and R. J. Mantz, "Wind Turbine Control Systems," *Advances in Industrial Control*, 2007.

[3] E. A. Bossanyi, "Wind Turbine Control for Load Reduction," *Wind Energy*, vol. 6, pp. 229-244, 2003.

[4] K. Johnson, L. Pao, M. Balas, and L. Fingersh, "Standard and Adaptive Techniques for Maximizing Energy Capture," *IEEE Control Systems Magazine*, Vol. 26, No. 3, pp. 70-81, 2006.

[5] E. A. Bossanyi, "Individual Blade Pitch Control for Load Reduction," *Wind Energy*, Vol. 6, pp. 119-128, 2003.

[6] E. A. Bossanyi, "Further load reductions with individual pitch control," *Wind Energy*, Vol. 8, pp. 481-485, 2005.

[7] S. Kanev and T. van Engelen, "Wind turbine extreme gust control," *Wind Energy*, Vol. 13, pp. 18-35, 2010.

[8] M. Jelavić, V. Petrović, and N Perić, "Estimation based Individual Pitch Control of Wind Turbine," *Automatika*, Vol. 51, pp. 181-192, 2010.

[9] M. Soltani, R. Wisniewski, P. Brath, and S. Boyd, "Load Reduction of Wind Turbines Using Receding Horizon Control," *IEEE International Conference on Control Applications*, 2011.

[10] J. Laks, L. Y. Pao, E. Simley, A. D. Wright, N. Kelley, and B. Jonkman, "Model Predictive Control Using Preview Measurements from LIDAR," *Proc. AIAA Aerospace Sciences Meeting*, 2011.

[11] F. Dunne, E. Simley, and L. Y. Pao, "LIDAR Wind Speed Measurement Analysis and Feed-Forward Blade Pitch Control for Load Mitigation in Wind Turbines," *National Renewable Energy Laboratory*, 2011.

[12] J. M. Jonkman and M. L. Buhl Jr., "FAST User's Guide," *National Renewable Energy Laboratory*, 2005.

[13] J. M. Jonkman, S. Butterfield, W. Musial, and G. Scott, "Definition of a 5-MW Reference Wind Turbine for Offshore System Development," *National Renewable Energy Laboratory*, 2009.

[14] M. O. L. Hansen, "Aerodynamics of Wind Turbines," *Earthscan*, 2. edition, 2008.

[15] G. Bir, "Multiblade Coordinate Transformation and Its Application to Wind Turbine Analysis," *ASME Wind Energy Symposium*, 2008.

[16] J. Laks, L. Pao, A. Wright, N. Kelley, and B. Jonkman, "Blade pitch control with preview wind measurements," *Proc. AIAA Aerospace Sciences Meeting*, 2010.

[17] E. Simley, L. Y. Pao, R. Frehlich, B. Jonkman, and N. Kelley, "Analysis of Wind Speed Measurements using Continuous Wave LIDAR for Wind Turbine Control," *Proc. AIAA Aerospace Sciences Meeting*, 2011.

[18] J. M. Maciejowski, "Predictive Control with Constraints," *Prentice Hall*, 1. edition, 2002.

[19] B. J. Jonkman, "TurbSim User's Guide," *National Renewable Energy Laboratory*, 2009.

[20] ASTM International, "Standard Practices for Cycle Counting in Fatigue Analysis", *ASTM E1049-85*, 2011.